

Inquiring the photocatalytic activity of cuprous oxide nanoparticles synthesized by a green route on methylene blue dye

Manoranjan Behera¹ · Gitisudha Giri¹

Received: 16 June 2015 / Accepted: 23 February 2016 / Published online: 17 March 2016
© The Author(s) 2016. This article is published with open access at Springerlink.com

Abstract We synthesized cuprous oxide (Cu_2O) nanoparticles (NPs) with an average crystallite size of 8.8 nm in presence of Arka (*Calotropis gigantea*) leaves extract. The photo-bleaching activity of Cu_2O NPs on the aqueous methylene blue (MB) dye was studied by illumination of visible light. In the absorption spectra, a decrease in the absorption peak intensity at 665 nm of MB was observed in presence of Cu_2O NPs. A red shift in its peak position as a function of irradiation time is suggesting that oxide particles are degrading the organic dye in an aqueous medium. In the vibration spectra, red shift in the C–H stretching band (2954, 2926, and 2855 cm^{-1}) of methylene group and C–N stretching band (1343 and 1226 cm^{-1}) of MB in presence of Cu_2O NPs proposes a surface adsorption of MB over NP's surfaces. Quenching in the emission band intensity and red shifts in the peak maxima of MB in presence of Cu_2O NPs is ascribed to the charge transfer interaction between MB and oxide NPs. A linear Stern–Volmer plot reveals that decrease in the emission intensity of MB dye occurs via the dynamic quenching mechanism. Synthesis of Cu_2O NPs of various architectures using a green route could be use as an approach towards the cost-effective treatment of water pollutants.

Keywords Photodegradation · Methylene blue dye · Surface adsorption · Charge transfer interaction · Photoluminescence quenching

Introduction

Organic dyes are the major threats to our environments. It is not an easy task to remove them from dye-bearing waste waters owing to their stability towards oxidizing agents [1–3]. Amongst the various organic dyes, methylene blue (MB)—a cationic dye mostly used in paper, rubber, and textile industry as colorants—is found in waste water [4–6]. It is reported that acute exposure to MB dye might cause tissue narcosis, heart stroke, jaundice, etc., in humans [7, 8]. Presently a variety of physical, chemical, and biological methods were available for the treatment of dye contaminated water. From an extensive literature study, we concluded that a chemical method such as adsorption process is an economical and efficient route for elimination of toxic dyes from polluted water [9–12]. In this regards, various low-cost adsorbents such as fly ash, metal sulfides (Ag_2S), and metal oxides (titania TiO_2 , cuprous oxide Cu_2O) have already been tested to treat polluted water [4, 9–13]. In recent years, semiconductor nanoparticles (NPs) were extensively used by scientists and academicians around the globe for the removal of various organic dyes via adsorption route. Pourahmad [4] reported that Ag_2S NPs encapsulated in a mesoporous material can efficiently degrade MB dye in aqueous solution. In another work, Srinivasan and White [13] reported an accelerated photodegradation of MB over three-dimensionally ordered macroporous TiO_2 pore sizes lies between 0.5 and $1\text{ }\mu\text{m}$. However, owing to high band gap of 3.2 eV, TiO_2 cannot perform in the visible region.

Among the various semiconductor metal oxides as photocatalyst, Cu_2O NPs find a special place in photocatalysis under visible light [10–12, 14–16]. Wide applications of this oxide NPs are mainly owing to its non-toxicity, easy availability of cheap and up-scalable

✉ Manoranjan Behera
mano.silicon@gmail.com

¹ Silicon Institute of Technology, Bhubaneswar, Odisha, India



synthetic routes, lying of the band gap (i.e., 2.17 eV) in the visible range, tunability of band gap, and strong tendency to adsorb molecular oxygen which helps in scavenging the photogenerated electrons so that electron–hole pairs recombination can be restrained easily at the interface [10–12, 14–16]. It is reported that size and shape are of paramount importance in tailoring the various properties and applications of the Cu₂O NPs. A variety of Cu₂O nanostructures such as wires, boxes, cubes, truncated cubes, octahedra, nanocages, nanomultipods, spheres, and a variety of hollow structures have already been synthesized and tested for their photocatalytic activity on various organic compounds [14, 15]. To develop diverse architectures of Cu₂O, the various methods widely used includes hydrothermal method, microemulsion method, surfactant-assisted route, and wet chemical method [10–12, 14–16]. Sun et al. [9] have reported an enhanced photocatalytic activity for Cu₂O–graphene oxide (GO) nanocomposite synthesized via solvothermal route towards Rhodamine B (RhB) dye. They reported that more than 65 % RhB was degraded within 80 min of visible light irradiation. Cai et al. [10] have reported synthesis of Cu₂O-reduced GO (rGO) composite by a one-pot hydrothermal method using glucose as reducing and cross-linking agent. They reported that as rGO promotes the charge carrier separation, it increases the aqueous photocatalytic efficiency. But, nearly 70 % methyl orange (MO) degradation was reported for this nanocomposite after a long irradiation time of 300 min. In another article, Zhang et al. [11] have reported 80 % MO degradation after 30 min irradiation by graphene/defected Cu₂O nanocomposite synthesized via a chemical vapor deposition method. They stressed on the importance of O-atoms towards the charge carrier separation. Zou et al. have reported synthesis of Cu₂O–rGO nanocomposites of various Cu₂O crystal facets. They have reported only 72, 60 and 28 % MB degradation after 120 min for octahedral, dodecahedral and cubic faceted Cu₂O–rGO NPs.

A few reports are available on photocatalytic activity study of Cu₂O NPs synthesized by green chemical route. Cu₂O microcrystals with well-formed facets were synthesized by a simple hydrothermal method by Zheng et al. [14] and investigated the surface stabilities and photocatalytic properties of the synthesized Cu₂O microcrystals. It is reported that Cu₂O {100} and {110} facets gradually disappear and transform into nanosheets during the photodegradation of MO dye. With the increase of irradiation time, Cu₂O microcrystals completely transform into nanosheets with {111} facets and the finally formed nanosheets exhibit stable photocatalytic activities. Zhu et al. [17] have synthesized Cu₂O micro-/nanocrystals using a simple liquid phase reduction process under microwave irradiation. In particular, for the dandelion

morphology, the photocatalytic degradation rates of RhB dye is reported to be highest, i.e., 56.37 %. From above literature studies we concluded that photodegradation efficiency of Cu₂O towards a dye depends on various parameters such as nature of the dye, synthesis route, shape and size of NPs, attachment of charge carrier separating agent to NP, adsorption capability, surface area, etc.

As we have not found any report on MB degradation by Cu₂O NPS obtained via a green route, in this manuscript we report on visible light photodegradation of MB dye by biosurfactant-capped Cu₂O NPs synthesized via a green route using leaves extract of Arka plant (i.e., *Calotropis gigantea*). The saponin molecules present in the plant extract not only acts as stabilizing agent [18] but is also believed to act as charge carrier separator. The synthesized nano-powders were characterized using UV–visible spectroscopy, Fourier transform infrared (FTIR) spectroscopy, X-ray photoelectron spectroscopy (XPS), X-ray diffraction (XRD), zeta potential, dynamic light scattering (DLS), photoluminescence (PL) spectroscopy, field emission scanning electron microscope (FESEM) and transmission electron microscope (TEM).

Experimental

Synthesis of Cu₂O NPs

We synthesized Cu₂O NPs by a green synthetic route using copper sulfate (CuSO₄·5H₂O) crystals as precursor salt, Arka leaves extract as encapsulating agent, and hydrazine hydrate as reducing agent in an aqueous medium. In an aim to synthesize Cu₂O NPs, first we prepared a precursor salt solution (1 M) by dissolving CuSO₄·5H₂O crystals in double-distilled water. After that, an aqueous plant extract was made by adding about 10 g of Arka leaves to 100 mL water in a conical flask and was boiled for 1 h in a hot plate. Now, the two solutions were mixed in a proper ratio and stirred in a magnetic stirrer for half an hour at 70 °C. Under the stirring condition, reducing agent was added dropwise till the blue color (i.e., due to Cu²⁺ ions) changed to a permanent reddish-brown suspension consisting of cuprous oxide (Cu₂O) NPs. The aqueous suspensions thus obtained was kept standstill overnight to settle down Cu₂O NPs. After careful decantation of upper supernatant liquid, those solid particles which were settled at the bottom of the container were kept in an electrical oven maintained at 80 °C for 2 h for complete removal of solvent so that samples can be collected in powder form. To confirm the formation of Cu₂O NPs, we added 2 mL of concentrated ammonia solution to 10 mg Cu₂O powders taken in a 25-mL beaker. A clear blue solution results from formation of [Cu(NH₃)₄(H₂O)₂]²⁺ complex after shaking the beaker



for a few seconds which indicates formation of copper(I) oxide [19]. The dried nano-powders were stored in desiccators for characterizations.

Characterization techniques

We characterized the as-synthesized Cu_2O powders using UV–visible spectroscopy, FTIR spectroscopy, XPS, XRD, zeta potential, DLS, PL spectroscopy, FESEM and TEM. UV–visible absorption spectra were acquired on a Perkin-Elmer spectrophotometer. The crystal phase of synthesized NPs was identified using an X-ray diffractometer (Rigaku D/Max 2000). Vibration spectra have been studied for the powder samples with a Thermo Nicolet Corporation FTIR Spectrometer (Model NEXUS-870). X-ray photoelectron spectrum (XPS) was collected on a VG ESCALAB MK-II spectrometer with a monochromatic Al $K\alpha$ source ($h\nu = 1486.6$ eV) operated at 10 kV and 20 mA at 10^{-9} Pa. Sample for XPS was prepared by drop-casting method. A drop of aqueous dispersion of Cu_2O NPs was placed on the silicon substrate and allowed to dry in desiccators by keeping overnight at room temperature. Zeta potential was measured using a Malvern Nano ZS instrument using phase analysis light scattering technique. Solid samples were sonicated for 20 min to well disperse oxide NPs in water prior to measuring zeta potential (ζ). The Malvern Nano ZS instrument was also used to find hydrodynamic diameter (D_h) of the aqueous suspension before and after adding Cu_2O NPs to MB dye. The dispersed samples were analyzed at least for thrice at 25 °C to get accurate results. The PL spectra have been recorded with a computer-controlled Perkin-Elmer (Model-LS 55) luminescence spectrometer in conjugation with a red-sensitive photomultiplier tube detector (RS928) and a high-energy pulsed Xe-discharge lamp as an excitation source (average power 7.3 W at 50 Hz). Image of a biosurfactant-modified Cu_2O nanocomposite powder was studied using FESEM of ZEISS SUPRA-40 and TEM of JEM-2100 (JEOL, Japan) machines. TEM sample was prepared by placing one drop of diluted solution on a carbon-coated 600-mesh copper grid and allowing the sample to dry in desiccators at room temperature. In the FESEM studies, the sample was spin-coated on a (110) silicon plate and then a thin gold coating was sputtered to make a conducting surface.

Photocatalytic degradation

To study the photodegradation of MB dye in an aqueous medium, first we prepared a suspension of Cu_2O particles (100 mg) by dispersing it in a 500 mL solution of MB (20 mg/L) in water. The aqueous suspension was then sonicated for 20 min in dark to make the powders disperse

well in the solution before irradiation with visible light. The photocatalytic reaction was conducted in a 500-mL cylindrical glass reactor. We used 500 W Xenon lamp with a UV cutoff filter as visible light source. The dispersion was bubbled with 100 mL/min O_2 and stirred magnetically at 30 °C. At regular intervals, 15 mL of the suspension was sampled and separated by centrifugation at 4000 rpm for 10 min to remove the powder. The concentration of residual MB (i.e., supernatant liquid) was measured by its absorbance (A) at 665 nm with a Perkin-Elmer spectrophotometer. The degradation efficiency (D) of MB was calculated using the equation, $D = (A_0 - A)/A_0 \times 100 \%$, where A_0 is the absorbance of 20 mg/L MB at 665 nm, A is the absorbance at the same wavelength of the extracted solution. As a control, another sample was analyzed without irradiating to test the adsorption ability of the oxide catalyst; other test methods were the same, as mentioned above.

Results and discussion

UV–visible spectra

Figure 1 shows evolution of absorption spectra (400–900 nm) of MB in presence of Cu_2O NPs upon irradiation of visible light; (a) 0, (b) 10, (c) 20, (d) 30, (e) 60, (f) 90, and (g) 120 min at room temperature. Before irradiating, MB solution with Cu_2O NPs was kept in the dark for nearly 3 h to eliminate possibility of other effects such as adsorption and reaction without light to affect the result. As shown in Fig. 1, MB displays two absorption bands, one near 605 nm and other one near 665 nm. The decrease in the intensity of absorption peaks with time elapsed is ascribed to degradation of MB by Cu_2O NPs. For

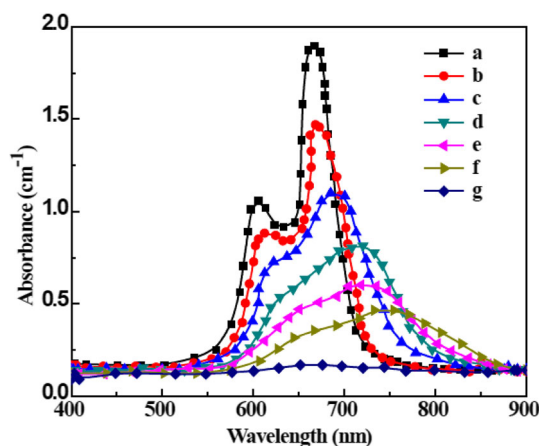


Fig. 1 Absorption spectra of MB in presence of Cu_2O NPs upon irradiation of visible light; a 0, b 10, c 20, d 30, e 60, f 90, and g 120 min



example, at 665 nm, the absorbance has decreased from 1.9 to 1.46 cm^{-1} after irradiation for only 10 min and this value has decreased to as small as 0.14 cm^{-1} after 120 min irradiation of visible light. This reveals that rate of decomposition of MB increases very fast with time. The extremely low intensity of 665 nm band after 120 min irradiation of light suggests that concentration of residual MB is very low.

We studied the degradation of MB to verify the photocatalytic activity of aqueous suspensions of Cu_2O NPs by irradiation with visible light. For this, we monitored the absorbance of MB solution at the absorption maximum wavelength 665 nm. The % degradation was calculated from the change in absorbance value during photodegradation with time of light irradiation. Figure 2 depicts the % degradation of MB before and after light irradiation against time of exposure. As can be seen from the Fig. 2, in the dark, the effect of photolysis on MB is not apparent. The concentration of MB solution slightly decreases due to the adsorption of MB on the surfaces of the catalyst. On the other hand, in presence of light, the %decomposition of MB dye in presence of Cu_2O NPs decreases non-linearly and reaches a value of 90 % after 120 min of light exposure. The observed photodegradation efficiency of biosurfactant-capped Cu_2O NPs on MB dye is due to presence of biosurfactant on its surface. The role of biosurfactant here is to promote charge carrier separation to enhance the photocatalytic efficiency. Cai et al. [10] have reported that the efficiency of Cu_2O NPs has increased owing to introduction of rGO which act as charge carrier separator. In comparison to the work by Zou et al. [12], our sample has performed well and may be ascribed to small size of the Cu_2O cluster as seen from TEM and FESEM images. In an article, Zho et al. [20] reported a similar decrease in the intensity of 665 nm band of MB by halloysite nanotube-

supported silver NPs. They have reported nearly 90 % of MB degradation after 60 min irradiation. They ascribed superior efficiency to larger surface area of halloysite nanotubes.

XRD pattern

Figure 3 depicts the XRD pattern of Cu_2O nanopowder (a) before and (b) after degrading MB dye. According to the JCPDS card no. 78-2076, both the patterns can be indexed as face-centered cubic structure [9–12]. Before adsorption of MB dye solution, the characteristic peaks (Fig. 3a) as observed at 2θ values of 29.3, 36.8, 42.3, 61.4, 73.5, and 77.6 are assigned to the crystal planes of (110), (111), (200), (220), (311), and (222) of crystalline Cu_2O , respectively [9–12]. From the most intense (111) peak, the crystallite size of Cu_2O NPs before and after MB adsorption is found to be 8.8 and 9.3 nm, respectively. The result implies that adsorption of MB dye on the surface of oxide particles hardly alters the crystallite size and the reclaimed Cu_2O NPs retain their catalytic activity.

FTIR spectra and DLS

Figure 4 which depicts vibration spectra in the ranges $3200\text{--}800\text{ cm}^{-1}$ for MB (a) before and (b) after adsorption on the Cu_2O NPs surface reveals photodegradation of the dye. As shown in Fig. 4a, the FTIR spectrum of MB shows three C–H stretching bands (2807 , 2866 , and 2924 cm^{-1}), one C–H bending vibration (920 cm^{-1}) and three C–N stretching bands (1131 , 1253 and 1352 cm^{-1}) [21–23]. After 60 min of light irradiation, a significant decrease in the intensities of these bands occurs when the MB dye gets adsorbed via S-atom on the surface of oxide NPs. Yu et al. [23] reported that the intensity of vibration bands between

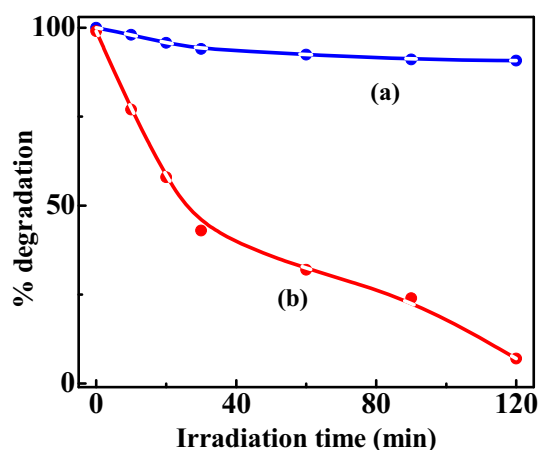


Fig. 2 Degradation of 20 mg/L MB in presence of Cu_2O NPs *a* before and *b* after visible light irradiation

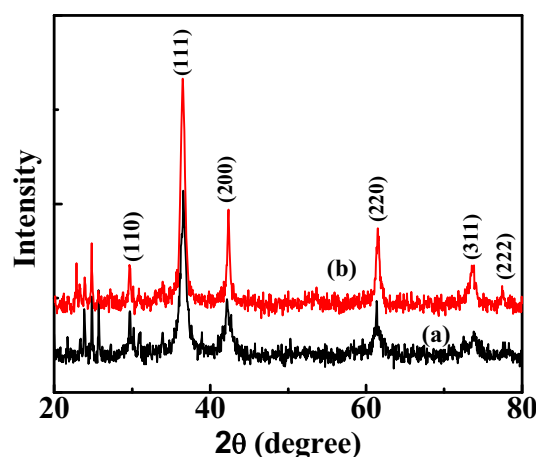


Fig. 3 XRD patterns of Cu_2O NPs *a* before and *b* after MB adsorption



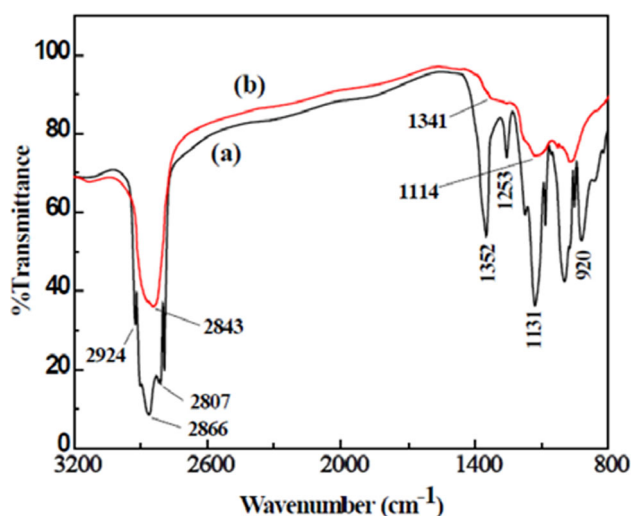


Fig. 4 FTIR spectra of MB *a* before and *b* after adsorption on Cu₂O NPs surface

1700 and 1100 cm^{-1} of MB dye has decreased in presence of TiO₂ NPs when illuminated with visible light. In another report, Amini et al. [24] showed that upon lighting with visible light, the intensity of C–N stretching band in MB dye has decreased drastically in presence of MnO_x/WO₃ catalyst and H₂O₂. A profound blue shift in these modes too indicates photodegradation of MB in presence of Cu₂O NPs via surface adsorption process. A large blue shift of nearly 23 cm^{-1} that is from 2866 to 2843 cm^{-1} in the C–H stretching band and nearly 3 cm^{-1} shift in C–N stretching bands suggests interfacial interaction between MB and oxide NPs. Disappearance of C–H bending vibration of heterocycle ring of MB in presence of oxide NPs also suggests that surface interaction arises between these two entities. In an experiment, Behera and Ram [25] have ascribed a small red shift of 5 cm^{-1} in the C=O stretching vibration in presence of Au NPs to a weak interaction between poly(vinyl pyrrolidone) polymer and Au surface via the O-atom of the pyrrolidone ring.

We also studied the size distributions of Cu₂O NPs (*a*) before and (*b*) after MB adsorption which are shown in Fig. 5. As it is seen from the DLS profile, the average hydrodynamic diameter of Cu₂O NPs has increased from 11.7 to 12.7 nm. This clearly hints that the average size of Cu₂O NPs has hardly increased when MB dye gets adsorbed on the oxide surface.

Zeta potential and XPS study

Figure 6 displays the distribution of zeta potential (ζ) of Cu₂O NPs (*a*) before and (*b*) after MB adsorption at 7.5 pH. As it is seen from the Fig. 6a, the zeta distribution profile of Cu₂O NPs before MB addition gives an average ζ -value

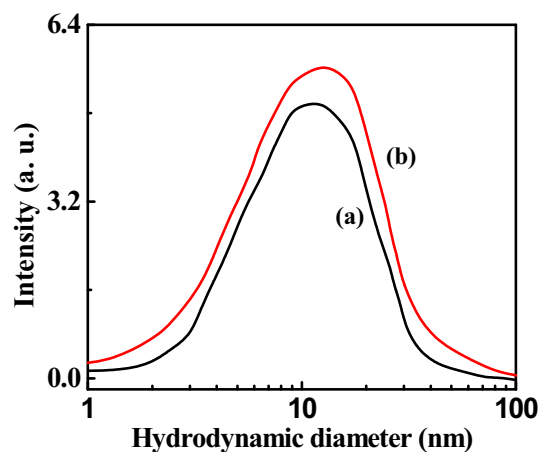


Fig. 5 Size distributions of Cu₂O NPs *a* before and *b* after MB adsorption in an aqueous dispersion

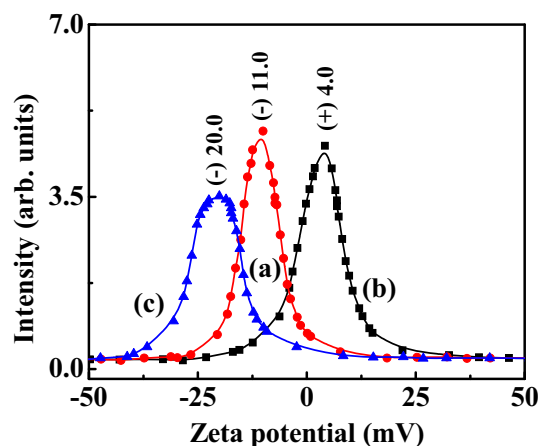
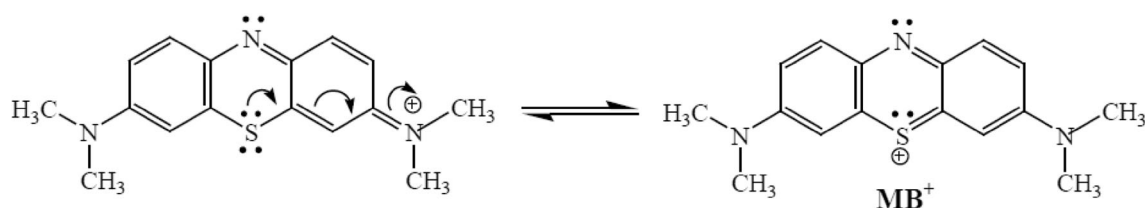


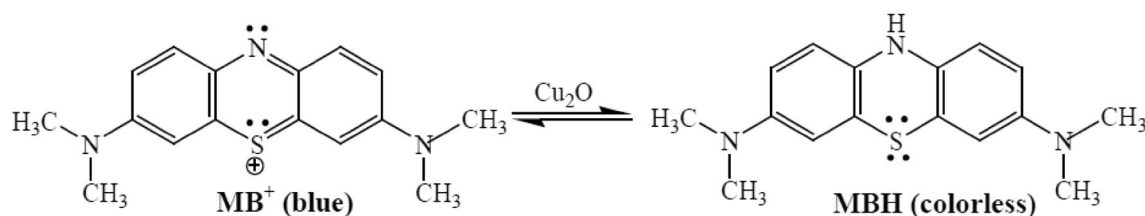
Fig. 6 Zeta potential distribution of Cu₂O NPs *a* before, *b* immediately after MB addition and *c* after 30 min of MB adsorption

(–) 11.0 mV. Negative zeta potential of Cu₂O NPs represents accumulation of negative charges on the surface of oxide NPs. When MB dye is added to the aqueous suspension of Cu₂O NPs and the ζ -value determined immediately, the sign has changed from negative to positive with an average ζ -value (+) 4.0 mV. The positive ζ -value could be ascribed to accumulation of positively charged S-atom of MB⁺ dye (see Scheme 1) on the surface of oxide NPs. After 30 min of illumination, the same sample again acquires a negatively charged surface with an average ζ -value (–) 20.0 mV. This may be ascribed to accumulation of negatively charged electrons on the oxide surface when donation of non-bonding electrons of S-atom of MBH (see Scheme 2) occurs to the surface of Cu₂O NPs [26]. Also it is observed from Table 1 that, when MB interacts with Cu₂O NPs, the full width at half maximum (FWHM), i.e., width of zeta band has increased from 9.8 to 11.0 mV. This value has further increased to a value 13.7 mV when it gets





Scheme 1 Structure of methylene blue



Scheme 2 Decolorization of methylene blue dye in presence of Cu_2O NPs

Table 1 Zeta potentials and full width at half maximum (FWHM) values for Cu_2O NPs before and after addition of MB dye

Samples	ζ -value (mV)	FWHM (mV)
(a) Cu_2O NPs before MB addition	(−) 11.0	9.8
(b) Cu_2O NPs immediately after MB addition	(+) 4.0	11.0
(c) Cu_2O NPs after 30 min of MB adsorption	(−) 20.0	13.7

adsorbed on the surface of oxide NPs. These results clearly hint that an interfacial interaction exists between MB and oxide NPs and extent of surface interaction increases with time. Yao and Wang [27] reported that the solution pH is an important parameter which controls the photodegradation efficiency of TiO_2 NPs on MB dye as it influences the sign of surface electrical charge of the oxide NPs. At pH 2, the average ζ -value of TiO_2 NP is reported to be (+) 19.04 mV whereas at pH 9, the average ζ -value of TiO_2 NP is (−) 25.49 mV.

XPS measurement was done to study the surface interaction between oxide NP and MB molecules and to finding the chemical state of copper (Cu) atom in synthesized NPs. Figure 6a depicts the XPS spectrum recorded for 2p photoelectrons of Cu (A) before and (B) after adsorption of MB molecules. In Fig. 6a, the XPS spectrum for Cu_2O NPs before MB adsorption detects a doublet for $\text{Cu}2p$ band, i.e., $\text{Cu } 2p_{3/2}$ and $\text{Cu } 2p_{1/2}$ at 932 and 952 eV, respectively [28]. In sample-B, i.e., after MB adsorption, the $\text{Cu } 2p_{3/2}$ band appears at binding energy (BE) of 932.9 eV. The band at 932.9 eV is assigned for $\text{Cu } 2p_{3/2}$ peak of Cu^0 . It is suggested that when Cu_2O NPs comes in contact with MB and irradiated with visible light, it oxidizes the dye and possibly itself gets reduced to Cu^0 from Cu^+ state. The $\text{O}1s$ peak of Cu_2O NPs before and after MB adsorption is shown in Fig. 6b. The broad peak which centered at 530.7 eV is for the metallic oxide (O^{2-}) [29]. Zhang et al. [11] have

reported $\text{O}1s$ peak of Cu_2O NPs at 531.94 eV owing to adsorbed O-atom. It is seen from the spectra that the intensity of this broad peak has drastically decreased in presence of MB. It may be ascribed to change in the chemical state of metallic oxide (O^{2-}) when MB molecules get adsorbed on the surface of oxide NPs. Lu et al. [30] reported that a clean Ti sample does not give an $\text{O}1s$ peak, but form a titanium oxide layer (O^{2-}) on the surface of Ti sample when exposed to excess oxygen, it results in a peak near 531.2 eV (Figs. 7, 8).

Photoluminescence study

Figure 9 shows the emission spectra (620–680 nm) of MB– Cu_2O dispersions consisting of (a) 0, (b) 1.0, (c) 2.0, (d) 3.0, (e) 5.0, and (f) 10.0 μM Cu_2O NPs in water, excited at 630 nm. As it is seen from Fig. 9, addition of 1 μM Cu_2O NPs caused only 18 % quenching of emission intensity of MB molecules and it has reached about 78 % after adding as large as 10 μM Cu_2O NPs. Such a noticeable decay in the emission intensity is ascribed to existence of a surface interaction between oxide NP and MB molecules as non-bonding electron (n) transfer occurs from S-atom of MBH molecules (see Scheme 2) to the surface of oxide NPs. Similar quenching in the emission intensity of various fluorophores was already reported in presence of an efficient light quencher like Au NP and ascribed to



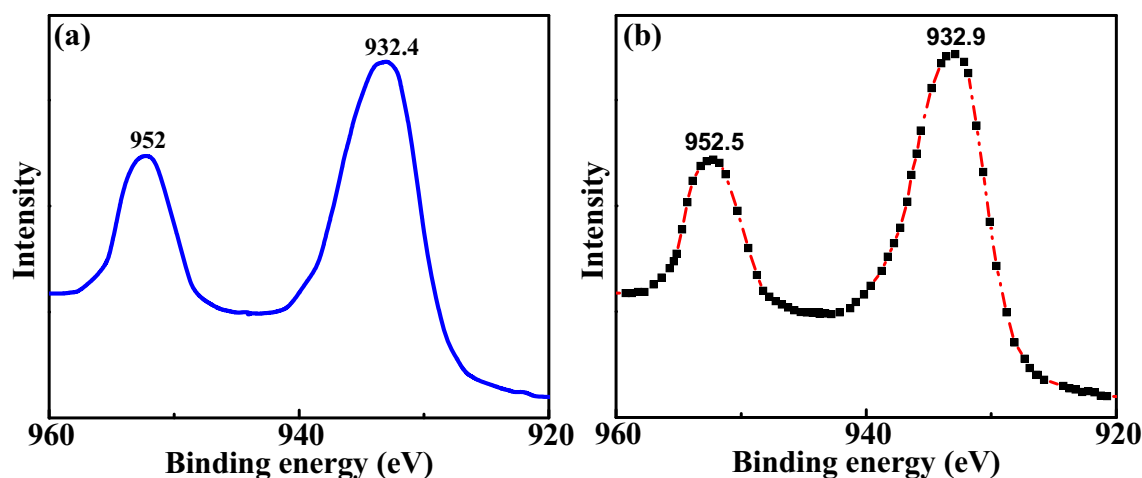


Fig. 7 XPS spectra ($\text{Cu}2p$ bands) of Cu_2O nanocrystals: **a** without and **b** with MB dye

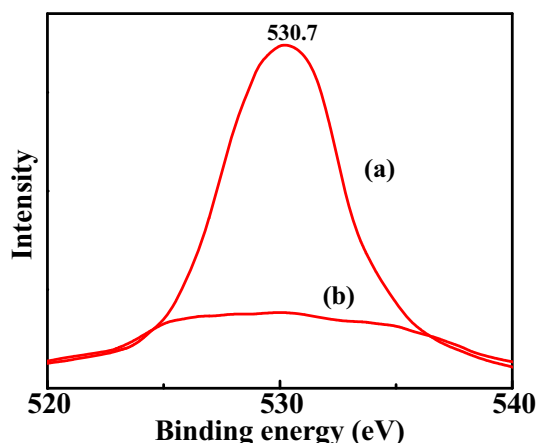


Fig. 8 XPS spectra ($\text{O}1s$ band) of Cu_2O nanocrystals: **a** before and **b** after MB dye adsorption

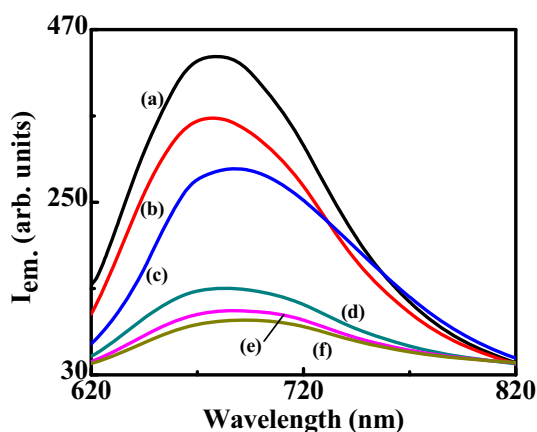


Fig. 9 Emission spectra of MB with different Cu_2O NPs content in water; **a** 0, **b** 1.0, **c** 2.0, **d** 3.0, **e** 5.0, and **f** 10.0 μM , excited at 630 nm

charge transfer interaction between these two moieties [31–34]. Zou et al. [12] have reported interfacial charge transfer process between different Cu_2O crystal facets and rGO sheets. They ascribed the strong PL quenching in case of octahedral Cu_2O /rGO crystal to a strong interfacial interaction between Cu_2O NPs and rGO sheets.

We also studied the variation of integrated emission intensity of MB molecules against Cu_2O contents and it is found that emission intensity of MB molecules have quenched intensely by addition of Cu_2O NPs (Fig. 10a).

Further we studied PL quenching of MB molecules in presence of an oxide quencher using the well-known Stern–Volmer equation [25, 34] which can be written as:

$$F_0/F = 1 + K_{SV}[Q] \quad (1)$$

where ' F_0 ' and ' F ' are the emission intensities of MB molecules in absence and presence of quencher (i.e., here it is Cu_2O NPs); $[Q]$ is the concentration of quencher (i.e., Cu_2O NP) and K_{SV} is quenching constant which tells about efficiency of a quencher. Figure 10b demonstrates the dependence of F_0/F on the concentration of Cu_2O NP. A linear relationship between F_0/F and Cu_2O NPs content as observed from the plot reveals that only one type of quenching occurs in the system [33, 34]. We obtained a K_{SV} value of $3.5 \times 10^5 \text{ M}^{-1}$ which can be obtained from the slope of the linear line. A linear Stern–Volmer plot reveals dynamic quenching mechanism in this system [32, 34]. Further, such a large K_{SV} value suggests existence of strong surface interaction between MB molecules and Cu_2O NP via S-atom of MBH molecule [32, 34, 35]. Tong et al. [35] have studied the interaction between MB dye and calf thymus deoxyribonucleic acid (ct-dRNA) by PL spectroscopic technique. In their study, they reported that



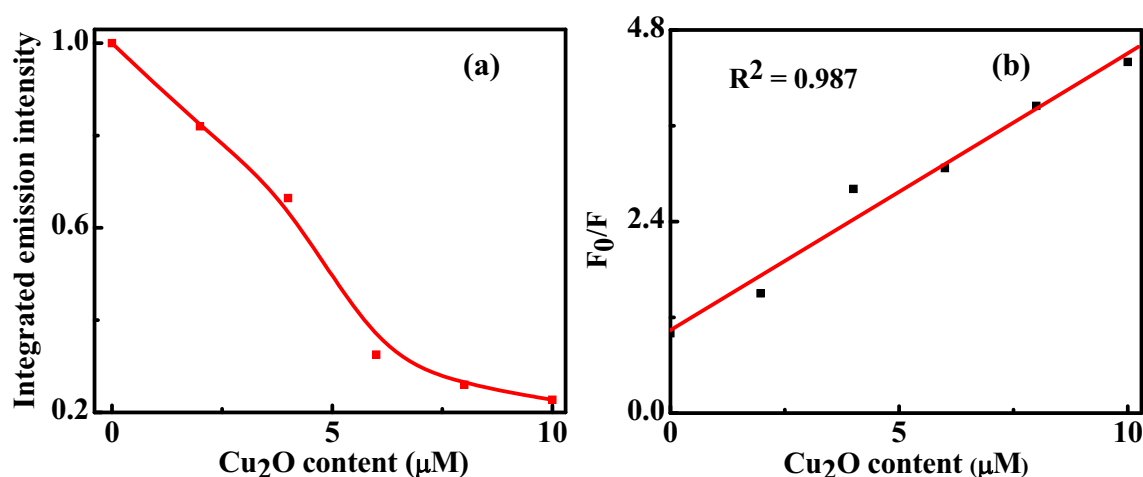


Fig. 10 **a** Variation of integrated emission intensity with Cu_2O content and **b** Stern–Volmer plot of F_0/F versus Cu_2O content. The linear fit gives $F_0/F = 1.04 + 0.35 [\text{Cu}_2\text{O}]$

upon addition of $55.6 \mu\text{M}$ ct-dRNA, the fluorescence intensity of MB can be quenched up to 80 % with no shifts in the emission wavelength owing to intercalation binding between MB and the ct-dRNA.

Microstructures

Morphologies of oxide NPs were studied from the FESEM and TEM images. In Fig. 11a, the SEM image shows nanoclusters of various architectures whose average diameters lies in the range of 5–15 nm. The TEM image in Fig. 11b from the same sample also illustrates nanoclusters of various shapes and sizes. An average size of 10 nm is estimated from the TEM image. Data are well supported by the DLS data (discussed in “FTIR spectra and DLS” section). Uniform distributions of Cu_2O NPs are observed from microscopic images. Zou et al. [12] have reported that

relatively larger size particle lie in the range of 200–400 nm for Cu_2O NPs of various shapes such as octahedral, dodecahedral and cubic crystals which were deposited on the surface of rGO.

Conclusions

We synthesized Cu_2O NPs using a green chemistry route and studied the photodegradation of MB dye in the visible region in presence of Cu_2O NPs in aqueous medium. Absorption spectra revealed that %decomposition of MB dye decreases non-linearly with Cu_2O contents and it reaches a value of 90 % after light exposure for 120 min. XRD result implies that adsorption of MB dye on the surface of oxide particles hardly alters the crystallite size. This implies that reclaimed Cu_2O NPs will maintain their

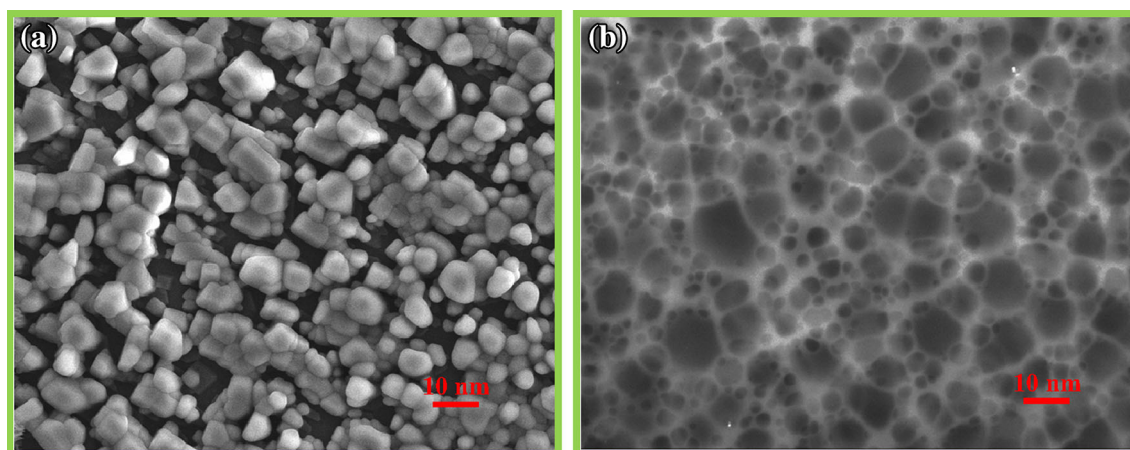


Fig. 11 **a** FESEM image and **b** TEM image of surfactant-capped Cu_2O NPs



original catalytic activity. XPS, FTIR, and zeta potential measurements suggest that an interfacial interaction which exists between MB dye and Cu₂O NPs is responsible for photodegradation of MB dye in presence of oxide NPs. Extensive quenching in the emission intensity of MB molecules in presence of Cu₂O NPs is ascribed to existence of a charge transfer-type interaction between oxide NP and MB molecules as transference of non-bonding electron (*n*) occurs from S-atom of MBH molecules to the surface of oxide NPs. A linear Stern–Volmer plot reveals existence of dynamic quenching mechanism in this system.

Acknowledgments Financial support of Silicon Institute of Technology is highly acknowledged.

Authors' contributions MB conceived the study, carried out all the experiments, and drafted the manuscript. GG helped MB in writing the manuscript. Both authors have read and approved the final manuscript.

Compliance with ethical standards

Conflict of interest The authors declare that they have no competing interests.

Open Access This article is distributed under the terms of the Creative Commons Attribution 4.0 International License (<http://creativecommons.org/licenses/by/4.0/>), which permits unrestricted use, distribution, and reproduction in any medium, provided you give appropriate credit to the original author(s) and the source, provide a link to the Creative Commons license, and indicate if changes were made.

References

- Kar A, Smith YR, Subramaniam V (2009) Improved photocatalytic degradation of textile dye using titanium dioxide nanotubes formed over titanium wires. *Environ Sci Technol* 43:3260
- Ma W, Li J, Tao X, He J, Xu Y, Yu JC, Zhao J (2003) efficient degradation of organic pollutants by using dioxygen activated by resin-exchanged iron(II) bipyridine under visible irradiation. *Angew Chem Int Ed* 42:1029
- Pal J, Ganguly M, Mondal C, Roy A, Negishi Y, Pal T (2013) Crystal-plane-dependent etching of cuprous oxide nanoparticles of varied shapes and their application in visible light photocatalysis. *J Phys Chem C* 117:24640
- Pourahmad A (2012) Ag₂S nanoparticle encapsulated in mesoporous material nanoparticles and its application for photocatalytic degradation of dye in aqueous solution. *Supperlattices Microstruct* 52:276
- Turhan K, Ozturkcan SA (2012) Decolorization and degradation of reactive dye in aqueous solution by ozonation in a semi-batch bubble column reactor. *Water Air Soil Pollut* 224:1353
- Salleh MAM, Mahmoud DK, Karim WAWA, Idris A (2011) Cationic and anionic dye adsorption by agricultural solid wastes: A comprehensive review. *Desalination* 280:1
- Nassar MM, Magdy YH (1997) Removal of different basic dyes from aqueous solutions by adsorption on palm-fruit bunch particles. *Chem Eng J* 66:223
- Vasanthkumar K, Ramamurthi V, Sivanesan SJ (2005) Modeling the mechanism involved during the sorption of methylene blue onto fly ash. *Colloid Interface Sci* 284:14
- Sun L, Wang G, Hao R, Han D, Cao S (2015) Solvothermal fabrication and enhanced visible light photocatalytic activity of Cu₂O-reduced graphene oxide composite microspheres for photodegradation of rhodamine B. *Appl Surf Sci* 358:91
- Cai J, Liu W, Li Z (2015) One-pot self-assembly of Cu₂O/RGO composite aerogel for aqueous photocatalysis. *Appl Surf Sci* 358:146
- Zhang D, Hu B, Guan D, Luo Z (2016) Essential roles of defects in pure graphene/Cu₂O photocatalyst. *Catal Commun* 76:7
- Zou W, Zhang L, Liu L, Wang X, Sun J, Wu S, Deng Y, Tang C, Gao F, Dong L (2016) Engineering the Cu₂O-reduced graphene oxide interface to enhance photocatalytic degradation of organic pollutants under visible light. *Appl Catal B Environ* 181:495
- Srinivasan M, White T (2007) Degradation of methylene blue by three-dimensionally ordered macroporous titania. *Environ Sci Technol* 41:4405
- Zheng Z, Huang B, Wang Z, Guo M, Qin X, Zhang X, Wang P, Dai Y (2009) Crystal faces of Cu₂O and their stabilities in photocatalytic reactions. *J Phys Chem C* 113:14448
- Zhang Y, Deneg B, Zhang T, Gao D, Xu AW (2010) Shape effects of Cu₂O polyhedral microcrystals on photocatalytic activity. *J Phys Chem C* 114:5073
- Abboud Y, Saffaz T, Chagraoui A, Bouari LL, Brouzi K, Tanane O, Ihsane B (2014) Biosynthesis, characterization and antimicrobial activity of copper oxide nanoparticles (CONPs) produced using brown alga extract (*Bifurcaria bifurcata*). *Appl Nanosci* 4:571
- Zhu Q, Zhang Y, Wang J, Zhou F, Chu P (2011) Microwave synthesis of cuprous oxide micro-/nanocrystals with different morphologies and photocatalytic activities. *J Mater Sci Technol* 27:289
- Behera M, Giri G (2014) Green synthesis and characterization of cuprous oxide nanoparticles in presence of a bio-surfactant. *Mater Sci Pol* 32:702
- Donnan FG, Thomas JS (1911) The solubility of cuprous oxide in aqueous ammonia solutions, and the composition of the cuprous-ammonia complex. *J Chem Soc Trans* 99:1788
- Zou M, Du M, Zhu H, Xu CS, Fu YQ (2012) Green synthesis of halloysite nanotubes supported Ag nanoparticles for photocatalytic decomposition of methylene blue. *J Phys D Appl Phys* 45:325302
- Ovchinnikov OV, Chernykh SV, Smirnov MS, Alpatova DV, Vorob'eva RP, Latyshev AN, Evlev AB, Utekhin AN, Lukin AN (2007) Analysis of interaction between the organic dye methylene blue and the surface of AgCl(I) microcrystals. *J Appl Spectrosc* 74:809
- Colthup NB, Daly LH, Wiberley SE (eds) (1990) Introduction to infrared and raman spectroscopy. Academic Press, Boston
- Yu Z, Chuang SSC (2007) Probing methylene blue photocatalytic degradation by adsorbed ethanol with in situ IR. *J Phys Chem C* 111:13813
- Amini M, Pourbadiei B, Purnima T, Ruberub A, Woob LK (2014) Catalytic activity of MnO_x/WO₃ nanoparticles: synthesis, structure characterization and oxidative degradation of methylene blue. *New J Chem* 38:1250
- Behera M, Ram S (2013) Spectroscopy-based study on the interaction between gold nanoparticle and poly (vinylpyrrolidone) molecules in a non-hydrocolloid. *Int Nano Lett* 3:17
- Anderson L, Wittkopp SM, Painter CJ, Lligel JJ, Schreiner R, Bell JA, Shakhasiri BZ (2012) What is happening when the blue bottle bleaches: An investigation of the methylene blue-catalyzed air oxidation of glucose. *J Chem Edu* 89:1425
- Yao J, Wang, C (2010) Decolorization of methylene blue with sol via UV irradiation photocatalytic degradation. *Int J Photoenergy*. Article ID 643182, 6



28. Yin M, Wu C, Lou Y, Burda C, Koberstein J, Zhu Y, O'briens S (2005) Copper oxide nanocrystals. *J Am Chem Soc* 127:9506
29. Heng B, Xiao OT, Tao W, Hu X, Chen X, Wang B, Sun D, Tang Y (2012) Zn doping-induced shape evolution of microcrystals: the case of cuprous oxide. *Cryst Growth Des* 12:3998
30. Lu G, Stevan LB, Jeffery S (2000) Oxidation of a polycrystalline titanium surface by oxygen and water. *Surf Sci* 458:80
31. Alexandridis P (2011) Gold nanoparticle synthesis, morphology control, and stabilization facilitated by functional polymers. *Chem Eng Technol* 34:15
32. Lakowicz JR (1999) Principles of fluorescence spectroscopy. Plenum Press, New York
33. Pramanik S, Banerjee P, Sarkar A, Bhattacharya SC (2008) Size-dependent interaction of gold nanoparticles with transport protein: a spectroscopic study. *J Lumin* 128:1969
34. Behera M, Ram S (2013) Intense quenching of fluorescence intensity of poly (vinyl pyrrolidone) molecules in presence of gold nanoparticles. *Appl Nanosci* 3:543
35. Tong C, Hu Z, Wu J (2010) Interaction between methylene blue and calfthymus deoxyribonucleic acid by spectroscopic technologies. *J Fluoresc* 20:261

